

# Global Biogeochemical Cycles<sup>®</sup>

## REVIEW ARTICLE

10.1029/2022GB007658

### Special Section:

REgional Carbon Cycle Assessment and Processes - 2

### Key Points:

- We synthesized estimates of river, lake and reservoir emissions of CO<sub>2</sub>, CH<sub>4</sub>, and N<sub>2</sub>O for 10 world regions and globally
- We re-estimate global inland water emission of 5.5 (3.5–9.1) Pg CO<sub>2</sub> yr<sup>-1</sup>, 100 (82–135) Tg CH<sub>4</sub> yr<sup>-1</sup>, and 322 (248–590) Gg N<sub>2</sub>O yr<sup>-1</sup>
- At 100 or 20 years horizon, CO<sub>2</sub> or CH<sub>4</sub> dominate global warming potential of emissions, respectively

### Supporting Information:

Supporting Information may be found in the online version of this article.

### Correspondence to:

R. Lauerwald,  
ronny.lauerwald@inrae.fr

### Citation:

Lauerwald, R., Allen, G. H., Deemer, B. R., Liu, S., Maavara, T., Raymond, P., et al. (2023). Inland water greenhouse gas budgets for RECCAP2: 2. Regionalization and homogenization of estimates. *Global Biogeochemical Cycles*, 37, e2022GB007658. <https://doi.org/10.1029/2022GB007658>

Received 26 NOV 2022










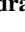
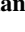
Accepted 19 APR 2023

### Author Contributions:

**Conceptualization:** Ronny Lauerwald, George H. Allen, Peter Raymond, Pierre Regnier

**Data curation:** Ronny Lauerwald, George H. Allen, Bridget R. Deemer, Shaoda Liu, Taylor Maavara, David Bastviken, Adam Hastie, Meredith A. Holgerson, Matthew S. Johnson, Bernhard Lehner, Alessandra Marzadri, Lishan Ran, Hanqin Tian, Xiao Yang, Yuanzhi Yao

## Inland Water Greenhouse Gas Budgets for RECCAP2: 2. Regionalization and Homogenization of Estimates

Ronny Lauerwald<sup>1</sup> , George H. Allen<sup>2</sup>, Bridget R. Deemer<sup>3</sup> , Shaoda Liu<sup>4,5</sup>, Taylor Maavara<sup>4,6,7</sup> , Peter Raymond<sup>4</sup> , Lewis Alcott<sup>7,8</sup>, David Bastviken<sup>9</sup> , Adam Hastie<sup>10,11</sup> , Meredith A. Holgerson<sup>12</sup> , Matthew S. Johnson<sup>13</sup> , Bernhard Lehner<sup>14</sup> , Peirong Lin<sup>15</sup>, Alessandra Marzadri<sup>16</sup>, Lishan Ran<sup>17</sup> , Hanqin Tian<sup>18</sup>, Xiao Yang<sup>19</sup>, Yuanzhi Yao<sup>20</sup> , and Pierre Regnier<sup>21</sup>

<sup>1</sup>Université Paris-Saclay, INRAE, AgroParisTech, UMR ECOSYS, Palaiseau, France, <sup>2</sup>Department of Geosciences, Virginia Polytechnic Institute and State University, Blacksburg, VA, USA, <sup>3</sup>U.S. Geological Survey, Southwest Biological Science Center, Flagstaff, AZ, USA, <sup>4</sup>Yale School of the Environment, Yale University, New Haven, CT, USA, <sup>5</sup>State Key Laboratory of Water Environment Simulation, School of Environment, Beijing Normal University, Beijing, China, <sup>6</sup>School of Geography, University of Leeds, Leeds, UK, <sup>7</sup>Yale Institute for Biospheric Studies, Yale University, New Haven, CT, USA, <sup>8</sup>Department of Earth & Planetary Sciences, Yale University, New Haven, CT, USA, <sup>9</sup>Department of Thematic Studies—Environmental Change, Linköping University, Linköping, Sweden, <sup>10</sup>School of GeoSciences, University of Edinburgh, Edinburgh, UK, <sup>11</sup>Carbon and Wetlands Group, Charles University, Prague, Czech Republic, <sup>12</sup>Department of Ecology and Evolutionary Biology, Cornell University, Ithaca, NY, USA, <sup>13</sup>Earth Science Division, NASA Ames Research Center, Moffett Field, CA, USA, <sup>14</sup>Department of Geography, McGill University, Montreal, QC, Canada, <sup>15</sup>School of Earth and Space Sciences, Institute of Remote Sensing and GIS, Peking University, Beijing, China, <sup>16</sup>Department of Civil, University of Trento, Environmental and Mechanical Engineering, Trento, Italy, <sup>17</sup>Department of Geography, The University of Hong Kong, Hong Kong, China, <sup>18</sup>Department of Earth and Environmental Sciences, Schiller Institute for Integrated Science and Society, Boston College, Chestnut Hill, MA, USA, <sup>19</sup>Department of Earth Sciences, Southern Methodist University, Dallas, TX, USA, <sup>20</sup>School of Geographic Sciences, East China Normal University, Shanghai, China, <sup>21</sup>Department Geoscience, Environment & Society—BGEOSYS, Université Libre de Bruxelles, Bruxelles, Belgium

**Abstract** Inland waters are important sources of the greenhouse gasses (GHGs) carbon dioxide (CO<sub>2</sub>), methane (CH<sub>4</sub>) and nitrous oxide (N<sub>2</sub>O) to the atmosphere. In the framework of the second phase of the REgional Carbon Cycle Assessment and Processes (RECCAP-2) initiative, we synthesize existing estimates of GHG emissions from streams, rivers, lakes and reservoirs, and homogenize them with regard to underlying global maps of water surface area distribution and the effects of seasonal ice cover. We then produce regionalized estimates of GHG emissions over 10 extensive land regions. According to our synthesis, inland water GHG emissions have a global warming potential of an equivalent emission of 13.5 (9.9–20.1) and 8.3 (5.7–12.7) Pg CO<sub>2</sub>-eq. yr<sup>-1</sup> at a 20 and 100 years horizon (GWP<sub>20</sub> and GWP<sub>100</sub>), respectively. Contributions of CO<sub>2</sub> dominate GWP<sub>100</sub>, with rivers being the largest emitter. For GWP<sub>20</sub>, lakes and rivers are equally important emitters, and the warming potential of CH<sub>4</sub> is more important than that of CO<sub>2</sub>. Contributions from N<sub>2</sub>O are about two orders of magnitude lower. Normalized to the area of RECCAP-2 regions, S-America and SE-Asia show the highest emission rates, dominated by riverine CO<sub>2</sub> emissions.

## 1. Introduction

As part of the first phase of the REgional Carbon Cycle Assessment and Processes (RECCAP) initiative (RECCAP-1), Raymond et al. (2013) re-estimated global inland water CO<sub>2</sub> evasion and presented the first ever maps of CO<sub>2</sub> emissions from streams and rivers as well as from lakes and reservoirs. Moreover, Raymond et al. demonstrated that inland water emissions have long been underestimated (e.g., Aufdenkampe et al., 2011; Cole et al., 2007) because small water bodies, which contribute over-proportionally to the overall emission flux, had been excluded. This publication became a milestone in the field, as it demonstrated the importance of inland waters for the global C budget.

Since RECCAP1, a growing number of global estimates of inland water greenhouse gas (GHG) emissions have been published, not only for CO<sub>2</sub> emissions (e.g., Holgerson & Raymond, 2016; Horgby et al., 2019; Lauerwald et al., 2015; Liu et al., 2022), but also for CH<sub>4</sub> (e.g., Holgerson & Raymond, 2016; Rosentreter et al., 2021; Stanley et al., 2016) and N<sub>2</sub>O (e.g., Hu et al., 2016; Lauerwald et al., 2019; Maavara et al., 2019; Marzadri et al., 2021; Soued et al., 2016; Yao et al., 2020), or for all three GHGs combined (e.g., Deemer et al., 2016;

**Formal analysis:** Ronny Lauerwald, George H. Allen, Bridget R. Deemer, Shaoda Liu, Taylor Maavara, Lewis Alcott, David Bastviken, Adam Hastie, Meredith A. Holgerson, Matthew S. Johnson, Alessandra Marzadri, Yuanzhi Yao

**Investigation:** Ronny Lauerwald, David Bastviken

**Methodology:** Ronny Lauerwald, George H. Allen, Bridget R. Deemer, Lewis Alcott, David Bastviken, Meredith A. Holgerson, Bernhard Lehner, Xiao Yang, Pierre Regnier

**Supervision:** Ronny Lauerwald, Pierre Regnier

**Validation:** Ronny Lauerwald, George H. Allen, Bridget R. Deemer

**Visualization:** Ronny Lauerwald, George H. Allen, Bridget R. Deemer, Lewis Alcott

**Writing – original draft:** Ronny Lauerwald, George H. Allen, Bridget R. Deemer, Shaoda Liu, Taylor Maavara, Peter Raymond, Lewis Alcott, David Bastviken, Adam Hastie, Meredith A. Holgerson, Matthew S. Johnson, Bernhard Lehner, Peirong Lin, Alessandra Marzadri, Lishan Ran, Hanqin Tian, Xiao Yang, Yuanzhi Yao, Pierre Regnier

**Writing – review & editing:** Ronny Lauerwald, George H. Allen, Bridget R. Deemer, Shaoda Liu, Taylor Maavara, Lewis Alcott, David Bastviken, Adam Hastie, Meredith A. Holgerson, Matthew S. Johnson, Bernhard Lehner, Peirong Lin, Alessandra Marzadri, Lishan Ran, Hanqin Tian, Xiao Yang, Yuanzhi Yao, Pierre Regnier

DelSontro et al., 2018). This development was supported by ongoing improvements with regard to quantity and quality of observational data. Most importantly, experimental research has been undertaken in regions which are potentially important for global inland water GHG budgets, but where observations had been extremely scarce—such as sub-Saharan Africa (Borges et al., 2015, 2019, 2022), SE Asia (Wit et al., 2015)) and Siberia (Karlsson et al., 2021; Serikova et al., 2019). Note for instance that older studies of GHG emissions from tropical lakes were not only highly uncertain because of the low number of observations, but also biased by largely using observations from unrepresentative systems such as floodplain lakes, as discussed by Borges et al. (2022), or reservoirs, as discussed by Lauerwald et al. (2019). Further, the transition from using CO<sub>2</sub> concentrations calculated from alkalinity and pH (as in Raymond et al., 2013), which are often biased where alkalinity is low and organic matter concentration is high (Abril et al., 2015), to using directly observed CO<sub>2</sub> emission rates (as in Liu et al., 2022), is a promising way to decrease uncertainties in inland water CO<sub>2</sub> emissions. In addition, global scale estimation of inland water GHG budgets have been improved through novel upscaling techniques based on statistical (e.g., DelSontro et al., 2018; Lauerwald et al., 2015; Liu et al., 2022) and process based models of varying complexity (e.g., Maavara et al., 2019; Yao et al., 2020). These upscaling techniques have been used to create gridded global maps of inland water emissions that allowed for the inclusion of inland waters in improved and spatially disaggregated, global GHG budgets (Bastos et al., 2020; Ciais et al., 2021; Stavert et al., 2022; Tian et al., 2020). However, previously published datasets and estimates differ largely with regard to the total global water surface area, which has been identified as one of the major persisting sources of uncertainties in global estimates of inland water GHG emissions (DelSontro et al., 2018). In a companion paper (Lauerwald et al., 2023a), we review these global estimates of inland water GHG emissions in detail.

Here, in the framework of the second phase of RECCAP (RECCAP-2), we present a synthesis of inland water GHG emissions based on these global estimates. Consistent with the overall objective of RECCAP-2 (Ciais et al., 2022), our synthesis covers inland water emissions of CO<sub>2</sub>, CH<sub>4</sub>, and N<sub>2</sub>O and breaks down existing estimates over 10 major world regions: North America (N-America), South America (S-America), Europe, Africa, Russia, West Asia (W-Asia), East Asia (E-Asia), South Asia (S-Asia), South-East (SE-Asia) and Australasia. Inland waters included in our synthesis comprise streams and rivers, as well as lakes and reservoirs. Note that smaller lentic water bodies such as ponds are not included in the synthesis due to lack of data regarding their global distribution. Further, temporally inundated floodplains and swamps are not included here, as those are wetlands which should be considered distinct from inland waters in GHG budgets.

We strive to give reasonable ranges of emission estimates at the global scale and for the 10 regions used in RECCAP-2, homogenizing existing estimates with regard to the assumed effective inland water surface area. For this, we make use of the most up-to-date datasets of inland water surface areas and estimates of seasonal ice-cover (Section 2). Then, based on existing estimates and collections of published, observed emission rates (as reviewed in Lauerwald et al., 2023a), we re-estimate the total emission of CO<sub>2</sub> (Section 3), CH<sub>4</sub> (Section 4), and N<sub>2</sub>O (Section 5) per type of inland water and per RECCAP-2 region. Finally, we present the full inland water GHG budget in terms of total warming potential at a 20 and 100 years time horizon (Section 6).

## 2. Homogenization of Existing Estimates

For our regionalized synthesis of inland water GHG emissions, we selected the most appropriate existing global estimates, complemented by a few regional assessments where appropriate (see details in Sections 4–6, and Lauerwald et al., 2023a). As mentioned before, we rescaled those estimates to consistent values of inland water surface area, accounting for the effects of seasonal ice-cover. In the following, we briefly describe the general methodology applied for this synthesis, starting with the general strategies to calculate area-normalized GHG flux rates for each estimate and RECCAP-2 region (Section 2.1). Then we describe the selected data Sets of inland water surface areas that were applied for this synthesis (Section 2.2), and how we corrected for effects of seasonal ice cover (Section 2.3).

### 2.1. Calculation of Area-Normalized Fluxes

Area-normalized fluxes were calculated in different ways, depending on the upscaling approach employed by each original study. For estimates based on direct empirical upscaling, where a global mean areal flux was applied to a global water surface area, the same areal flux was applied here to each of the 10 RECCAP-2 regions,

multiplying by the water surface area used in this synthesis. For binned upscaling, where this form of upscaling was performed for individual waterbody size classes (e.g., Holgerson & Raymond, 2016; Rosentreter et al., 2021) or latitude bins (e.g., Bastviken et al., 2011; Harrison et al., 2021; Marzadri et al., 2021; Rosentreter et al., 2021), the same bins were used, multiplying originally reported mean areal fluxes by the surface area of each bin calculated in this study. Finally, spatially explicit estimates of areal GHG fluxes (as for instance Stavert et al., 2022 and Johnson et al., 2021) were averaged by RECCAP-2 region, and then multiplied by the surface area used for our synthesis. However, where GHG emissions are simulated with process-based, biogeochemical models, emission estimates scale to simulated biogeochemical transformation fluxes and are rather independent of the assumed water surface area (see for instance Lauerwald et al., 2017). This is the case for model-based estimates of CH<sub>4</sub> (Johnson et al., 2021, 2022), N<sub>2</sub>O (Lauerwald et al., 2019; Maavara et al., 2019; Yao et al., 2020) and CO<sub>2</sub> (Tian et al., 2015). Here, we aggregated the original flux estimates directly per RECCAP-2 region. Details on which estimates were used for our regionalized synthesis, and which type of areal-homogenization was applied is given in the following three sections for CO<sub>2</sub> (3), CH<sub>4</sub> (4), and N<sub>2</sub>O (5).

## 2.2. Water Surface Data Used in This Synthesis

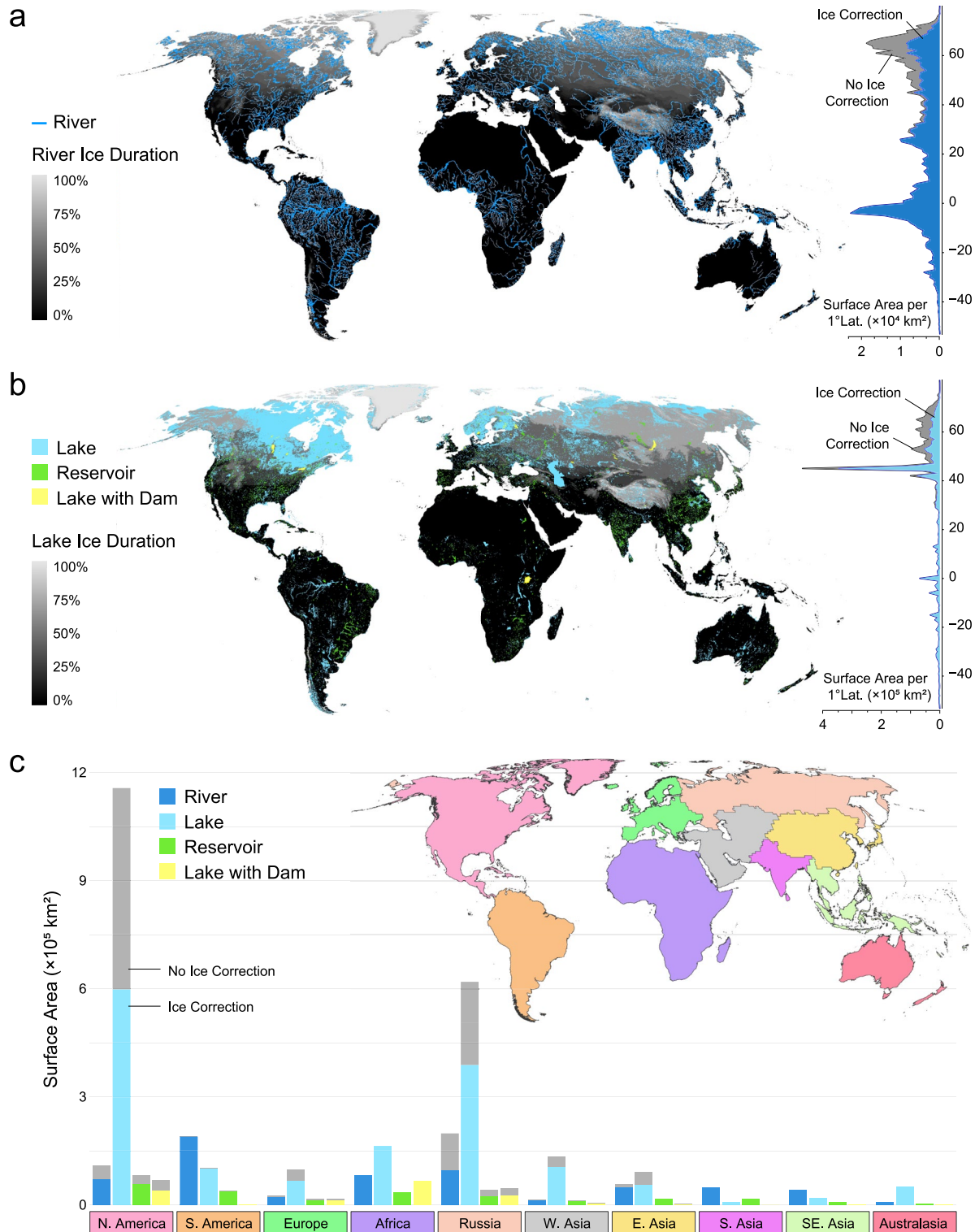
For rivers, the primary source of surface area comes from the GRWL database v.1.0 (Allen & Pavelsky, 2018) (Figure 1a), which we consider the best-available data set for that purpose (see, Lauerwald et al., 2023a for further details). Following the approach presented in Allen and Pavelsky (2018), we calculate the total global river surface area as 773,000 km<sup>2</sup>, excluding the effects of seasonal ice cover. In this approach, the surface area of rivers and streams narrower than 90 m was estimated by developing basin-specific statistical distributions of river widths in large rivers and extrapolating these widths to narrower rivers and streams (Allen & Pavelsky, 2018). As seen in Figure 1a, a large amount of river surface area is concentrated in the tropics and the Arctic, particularly if the impact of river ice is not taken into consideration.

For lake and reservoir surface area, we use data from HydroLAKES v.1.1 (Messenger et al., 2016). HydroLAKES contains only water bodies larger than 0.1 km<sup>2</sup> and is thus rather conservative with regard to total lake and reservoir surface area. We prefer these rather conservative estimates over remote-sensing-based products like GloWaBo (Verpoorter et al., 2014) which was evaluated only against national inventory data for Sweden and is prone to contamination with wrongly attributed surface areas (Pi et al., 2022), in particular as non-supervised classification algorithms have been applied. More importantly, HydroLAKES classifies each water body as a natural lake, a reservoir, or a natural lake with a dam (e.g., Lake Victoria in Figure 1b). The distinction between natural lakes and reservoirs is important, as we partly deal with distinct areal flux rates for both types of standing water bodies. For each of the three lake types distinguished in HydroLAKES, we sum water surface area in each of the 10 RECCAP-2 regions (Figure 1c). Excluding the effects of ice cover and water bodies with a surface area less than 0.1 km<sup>2</sup>, the total surface area of natural lakes is 2,442,443 km<sup>2</sup>, reservoirs is 266,894 km<sup>2</sup>, and lakes with a dam is 209,474 km<sup>2</sup>, for a grand total of 2,918,811 km<sup>2</sup>.

Some of the GHG emission estimates we synthesized give estimates per latitudinal bands and/or per stream order (see Section 3–5). To provide useful input for rescaling those estimates to the river surface area used for this study, we partitioned the stream surface area accordingly. For stream order, we determine the surface area of rivers and streams with a Horton-Stahler stream order  $\leq 3$  and stream order  $> 3$ . To accomplish this task, we use the HydroSHEDS-based RiverATLAS version 1.0 data set (Linke et al., 2019), which contains the stream order and an estimated river surface area for each river segment based on hydraulic geometry relationships from Allen et al. (1994). For each RECCAP-2 region, we calculate the proportion of surface area of rivers and streams in RiverATLAS in each stream order category and then apply this proportion to the surface area of each RECCAP-2 region derived from Allen and Pavelsky (2018). Estimates of areal proportions of different lake size classes were obtained based on the attribute data stored in the HydroLAKES v.1.1 database.

## 2.3. Correction for Effects of Ice-Cover

We account for the effects of river ice by reducing the amount of river surface area by the proportion of the year that rivers are covered by ice (Figure 1a). We estimate ice duration using the river ice model presented by Yang et al. (2020). The model uses a logistic regression equation to estimate river ice probability from the mean surface air temperature and considers the difference between freeze-up and breakup processes. Surface air temperature



**Figure 1.** Global surface area of inland water bodies. (a) River surface area with ice duration correction. (b) Lake, Reservoir, and Lake with dam surface area with ice duration correction. (c) Water body surface area within each of the 10 RECCAP-2 regions. Insets in panels a and b report the latitudinal distribution of water surface area without/with ice correction.

inputs to the river ice model are from ERA5 climate reanalysis daily aggregated data from 2010-07 to 2020-07 (<https://cds.climate.copernicus.eu/>). Each daily probability ( $[0-1]$ ) map is then converted to binary “ice-cover” ( $\geq 0.5$ ) or “ice-free” ( $< 0.5$ ) map, before all the daily binary rasters are temporally averaged across the 10-year study period to arrive at the 10-year river ice occurrence raster (Figure 1a). The GRWL-based river surface area measurements are then scaled by the proportion of the year that rivers are ice free. The ice correction reduces the global effective surface area of rivers and streams to 616,000 km<sup>2</sup> (a relative decrease of 20.3%) and is particularly important in N-America and Russia, where river ice is most prevalent (Figure 1c).

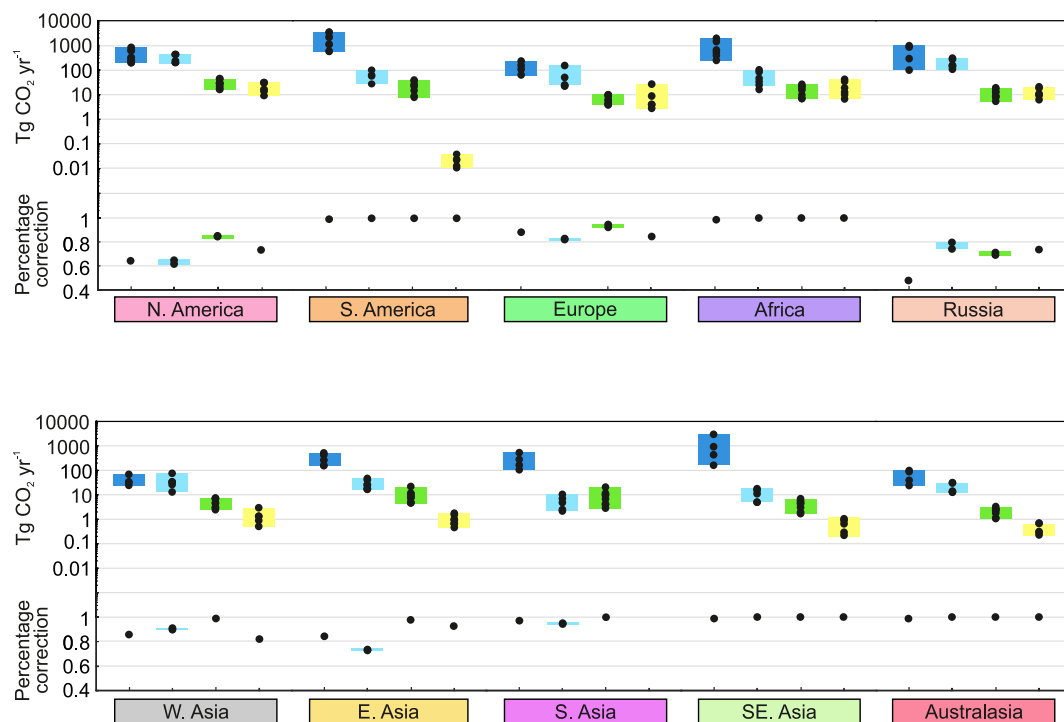
To account for the effect of ice cover on lakes and reservoirs during the winter months, we multiply the surface area of each lake and reservoir by the average proportion of the year that the waterbody remains ice free (Figure 1b). We estimate lake and reservoir ice duration using monthly surface air temperatures from 1970 to 2000 from WorldClim 2 (Fick & Hijmans, 2017). For each lake and reservoir, we determine the proportion of the year that surface air temperatures are below 0°C, an isothermic threshold that is a good predictor of lake ice occurrence (Murfitt & Brown, 2017; Sharma et al., 2019; Weyhenmeyer et al., 2004). Applying the ice cover correction reduces the global effective surface area of natural lakes to 1,553,842 km<sup>2</sup> (a relative decrease of 36.4%), reservoirs to 219,082 km<sup>2</sup> (17.9%), and lakes with a dam to 154,610 km<sup>2</sup> (26.2%), for a grand total effective surface area of 1,927,534 km<sup>2</sup> (34.0%). Much of this reduction occurs in natural lakes located in the Canadian Shield and in Siberia corresponding to RECCAP-2 regions N-America and Russia (Figure 1c).

Spring ice melt is associated with a pulse of CH<sub>4</sub> and CO<sub>2</sub> emissions from lakes and reservoirs (Denfeld et al., 2018). Specifically, Denfeld et al. (2018) estimates that 17% of annual emissions of carbon dioxide and 27% of annual emissions of methane occur during this ice-off period in lakes and reservoirs. Thus, for lakes and reservoirs that freeze, we applied as well a corresponding ice-melt correction factor for CO<sub>2</sub> and CH<sub>4</sub>, which lowers the overall impact of seasonal ice cover. This should be noted as a simplification based on studies of a limited number of individual systems, not accounting for their representativity in terms of system characteristics or ice period length. While there is preliminary evidence that a similar ice-off flux of N<sub>2</sub>O may take place in some northern lakes (Cavaliere & Baulch, 2018), there remains insufficient field data as well as mechanistic understanding of under-ice N<sub>2</sub>O production processes to scale this process to any of the RECCAP-2 regions or globally. Thus, inland water N<sub>2</sub>O emission is only corrected for by rescaling fluxes to relative length of ice-free period.

### 3. Inland Water CO<sub>2</sub> Budget

In our companion paper presenting a review on existing global inland water GHG budgets (Lauerwald et al., 2023a), we identified global water surface area as a major factor of uncertainty explaining a large proportion of differences between estimates. In this synthesis, we remove that factor of inconsistency and standardize all flux estimates reviewed in Lauerwald et al. (2023a) to the same data set of inland water surface area (Allen & Pavelsky, 2018; Messager et al., 2016) and apply the same procedure of correction of seasonal ice-cover as explained in Section 2.3. The rescaled emission estimates from the individual studies retained for that synthesis are listed in Table S1. Most of these estimates are global, spatially explicit estimates covering all regions (Raymond et al., 2013; Lauerwald et al., 2015; Liu et al., 2022, and simulation results from DLEM), which were complemented by regional estimates covering only one (Borges et al., 2015, 2022; Butman & Raymond, 2011; Li et al., 2018; Ran et al., 2021) or two regions (Hastie et al., 2018). For standardizing the studies by St. Louis et al. (2000), Deemer et al. (2016), and DelSontro et al. (2018) that are based on a robust database of observations but only give a lumped global estimate, we simply applied the same average emission rate to the ice-corrected water surface area of the corresponding water body type in each RECCAP-2 region.

Note that following DelSontro et al. (2018), we used two average emission rates for this study, one simply based on the mean of observations, and one derived from statistical upscaling based on assumed statistical distributions of phosphorus concentrations and water body size. Using the lake size distribution from HydroLAKES, the second emission rate (277 g CO<sub>2</sub> m<sup>-2</sup> yr<sup>-1</sup>) based on statistical upscaling is less than half of the rate derived from the arithmetic mean of observations (615 g CO<sub>2</sub> m<sup>-2</sup> yr<sup>-1</sup>). Although the statistical function used by DelSontro et al. (2018) has a low R<sup>2</sup> of 0.11 and upscaling results are thus not necessarily robust, the large difference between both rates indicates that the observational basis is not necessarily representative for global lakes, suggesting that direct upscaling of observations might lead to strong overestimations. This can further be explained by an underrepresentation of large, tropical lakes that tend to have both a lower productivity and lower CO<sub>2</sub> emissions than temperate or boreal lakes (see Figure 7 in Borges et al., 2022). We thus retained both rates for

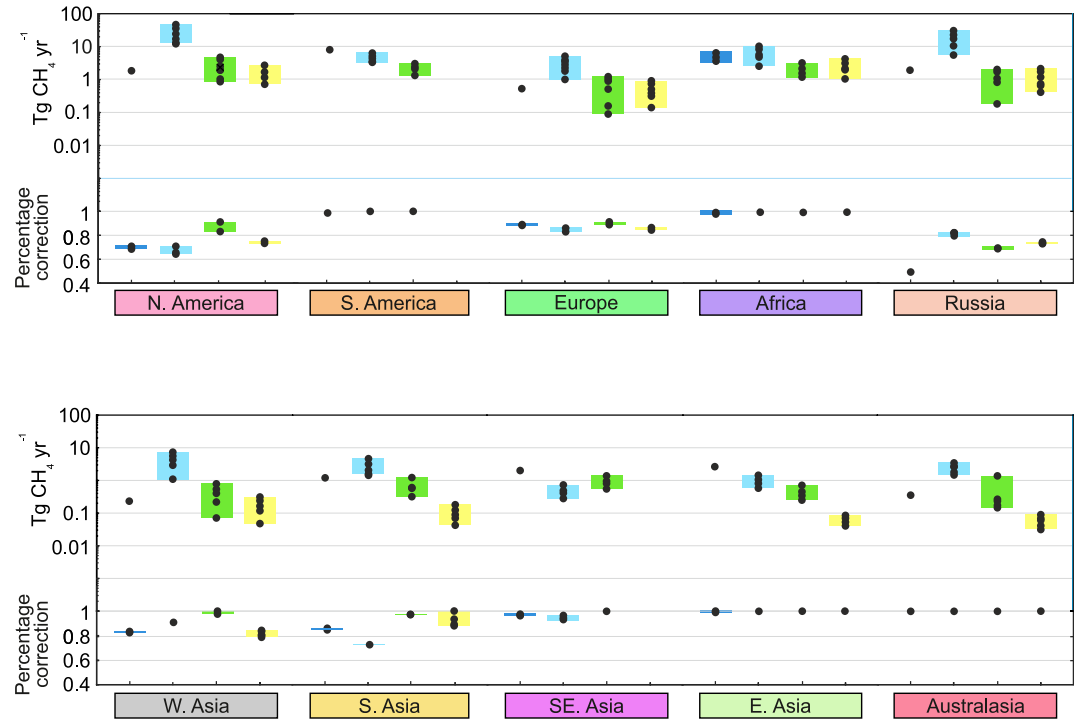


**Figure 2.** Spatial and statistical distribution of standardized inland water CO<sub>2</sub> emission flux. Regional estimates of CO<sub>2</sub> emission (Tg CO<sub>2</sub>-C yr<sup>-1</sup>) in the top bars, ice-corrected surface area estimates in blue lines, and the percent change in total annual emission from the combination of ice and ice melt corrections in the bottom bars. Regional emissions are shown from rivers (dark blue), natural lakes (light blue), reservoirs (green) and lakes with a dam (yellow). Each black dot represents the regionalized emission from one study in the literature, such that the bars show the range of regionalized emissions across studies. More detailed information on the individual flux estimates can be found in Table S1.

our analysis, as lower and upper bound values derived from the same observational data set, the range reflecting the huge uncertainty arising from distinct upscaling methods. For standardizing the estimates by Holgerson and Raymond (2016), we applied the reported average emission rates for four lake size classes (0.1–1 km<sup>2</sup>, 1–10 km<sup>2</sup>, 10–100 km<sup>2</sup>, >100 km<sup>2</sup>). For the estimates by Harrison et al. (2021), we used average emission rates for four latitudinal bands (0–25, 25–54, 54–66, >66° latitude). Figure 2 shows the ranges of all standardized estimates per water body type and RECCAP-2 region. It also reports the correction factors that were applied to account for seasonal ice cover and the emission pulse during spring ice melt.

If we sum up the median (min-max) values of surface-area homogenized estimates per RECCAP-2 region over the globe, we obtain CO<sub>2</sub> evasion fluxes of 4.49 (1.65–11.56) Pg CO<sub>2</sub> yr<sup>-1</sup> for streams and rivers, 0.70 (range: 0.43–1.29) Pg CO<sub>2</sub> yr<sup>-1</sup> for lakes, 0.11 (range: 0.05–0.20) Pg CO<sub>2</sub> yr<sup>-1</sup> for reservoirs, respectively (see Table S2 in Supporting Information S2). Lakes regulated by dams as third lake type contribute another 0.06 (range: 0.03–0.13) Pg CO<sub>2</sub> yr<sup>-1</sup>. When we aggregate these estimates to assess the total global inland water CO<sub>2</sub> emissions, we have to account for all possible combinations of individual estimates. If we sum up all median values (interquartile range - IQR) of all possible combinations per RECCAP-2 region, we calculate an emission of 5.55 (IQR: 3.50–9.08) Pg CO<sub>2</sub> yr<sup>-1</sup>. Streams and rivers are the largest contributor to the global aquatic CO<sub>2</sub> evasion (~84%), despite a surface area of only 1/5 that of global lakes, but with average emission rates about one order of magnitude higher than those of lakes and reservoirs (see Lauerwald et al., 2023a). In comparison, lakes and reservoirs make up only 13% and 2% of the total aquatic evasion, respectively. Globally, seasonal ice coverage that is partly counterbalanced by peak emissions during ice melt still removes 18% of estimated annual CO<sub>2</sub> emissions from inland waters. The most important reductions are estimated, not surprisingly, for Russia (46%) and N-America (35%).

Across the RECCAP-2 regions, S-America has the highest aquatic CO<sub>2</sub> evasion (1.72 Pg CO<sub>2</sub> yr<sup>-1</sup>), followed by Africa, SE-Asia, Russia and N-America (0.68–0.80 Pg CO<sub>2</sub> yr<sup>-1</sup>, all median estimates, see Table S2 in Supporting Information S2). In contrast, Australasia and the W-Asia have the lowest aquatic CO<sub>2</sub> evasion among the



**Figure 3.** Spatial and statistical distribution of standardized inland water  $\text{CH}_4$  emission flux. Regional estimates of methane emission ( $\text{Tg CH}_4 \text{ yr}^{-1}$ ) in the top bars, ice-corrected surface area estimates in blue lines, and the percent change in total annual emission from the combination of ice and ice melt corrections in the bottom bars. Regional emissions are shown from rivers (dark blue), natural lakes (light blue), reservoirs (green) and lakes with a dam (yellow). Each black dot represents the regionalized emission from one study in the literature, such that the bars show the range of regionalized emissions across studies. More detailed information on the individual flux estimates can be found in Table S1.

RECCAP-2 regions (median estimates of  $0.07\text{--}0.09 \text{ Pg CO}_2 \text{ yr}^{-1}$ ). In most RECCAP-2 regions, rivers are the dominant contributor to aquatic  $\text{CO}_2$  emissions. Exceptions are N-America and W-Asia, where they contribute only half of the emissions flux, due to the fact that in these regions the inland water surface area is strongly dominated by lakes (see Figure 2). In contrast, in S-America, S- and SE-Asia, standing waters contribute less than 5% to the estimated inland water  $\text{CO}_2$  emission.

#### 4. Inland Water $\text{CH}_4$ Budget

In this synthesis, we calculate total area-normalized  $\text{CH}_4$  fluxes from each study reviewed in the companion paper by Lauerwald et al. (2023a), considering both diffusive and ebullitive pathways but excluding plant-mediated fluxes (as in Bastviken et al., 2011) and reservoir turbine degassing (as in Harrison et al., 2021). The individual results of this area-normalization are listed in Table S1, based on which Figure 3 gives an overview of value ranges and the effect of correction for seasonal ice-cover. However, when summarizing regionalized aquatic  $\text{CH}_4$  emissions, we do not include emission estimates from older studies that incorporated unrealistic areal coverages and small sample sizes of observed emission rates (reservoir fluxes from St. Louis et al., 2000 and river fluxes from Bastviken et al., 2011).

Among the studies retained for the regionalization and homogenisation of methane emission from standing water bodies, there are two studies that were based on direct upscaling (Deemer et al., 2016; DelSontro et al., 2018), four studies based on binned upscaling (Bastviken et al., 2011; Harrison et al., 2021; Holgersson & Raymond, 2016; Rosentreter et al., 2021), and finally three gridded estimates (Johnson et al., 2021, 2022; Stavert et al., 2022). For rivers we only retained the estimate based on the binned upscaling by Rosentreter et al. (2021). Depending on the spatial resolution of the original studies (global, binned, regionalized, gridded), estimates were rescaled to a homogenized data set of total and effective (i.e., corrected for effects of seasonal ice-cover and ice melt) water surface area as described in Section 2. Note that for two studies (Harrison et al., 2021; Johnson et al., 2021),

which included a correction of seasonal ice-cover, we were not able to disentangle the ice-correction from areal emission rates. In these two cases, instead of applying our own correction, we adopted the ice-correction from the original studies. Finally, we included three regional estimates in our analysis: the studies by Borges et al. (2015) and Borges et al. (2022) that give estimates for African rivers and lakes, respectively, and the study by Li et al. (2018) that gives estimates for lakes and reservoirs in China. In the latter case, we extrapolated the average flux rates over the whole of RECCAP-2 region E-Asia, which besides China further includes the two Koreas and Japan.

Aside from wetlands (not examined here), lakes are the single largest source of inland water methane emissions, emitting a median (min-max) of 59.6 (29.5–115.7) Tg CH<sub>4</sub> yr<sup>-1</sup> followed by rivers with 22.9 Tg CH<sub>4</sub> yr<sup>-1</sup>, and reservoirs with a median (min-max) emission of 11.6 (4.8–18.7) Tg CH<sub>4</sub> yr<sup>-1</sup> (see Table S3 in Supporting Information S2). Lakes with dams, which we consider here separately as a third category of standing water bodies following Messenger et al. (2016), contribute a median (min-max) emission of 6.2 (2.4–10.9) Tg CH<sub>4</sub> yr<sup>-1</sup>. For standing water bodies, area-homogenisation has slightly reduced the spread in estimates from a factor 4–5 (Lauerwald et al., 2023a) to a factor 3–4 (Table S3 in Supporting Information S2). The dominance of lake emissions is the most prominent in Regions N-America, Russia, W-Asia and Australasia where they contribute about 80% to inland water CH<sub>4</sub> emissions (see Figure 3 and Table S3 in Supporting Information S2). While the dominance of lakes in methane emissions holds for the majority of regions, the large surface area of rivers in S-America, S- and SE-Asia result in river methane emissions that rival or exceed lake emissions. In these same three regions, reservoirs constitute a high fraction of lentic water bodies (and methane emissions). Africa also has a high fraction of its freshwater methane emissions coming from lakes with a dam, of which Lake Victoria as Africa's largest lake is the most prominent example.

When combining these rescaled estimates to re-assess the total global inland water CH<sub>4</sub> emission, we have again a large number of possible combinations. If we calculate median values (and interquartile ranges - IQR) of all possible combinations of estimates covering all types of inland waters per RECCAP-2 region (see Table S3 in Supporting Information S2) and sum those up, we obtain a global inland water CH<sub>4</sub> evasion flux estimate of 100.3 (IQR: 82.1–134.8), which is at the lower end of the range of estimates reported in AR6 of the IPCC (112–217 Tg CH<sub>4</sub> yr<sup>-1</sup>). Highest inland water CH<sub>4</sub> emissions of 27.5 (IQR: 19.8–41.5) and 17.9 (IQR: 13.8–29.4) Tg CH<sub>4</sub> yr<sup>-1</sup> are estimated respectively for N-America and Russia, which together cover more than two thirds of total lake surface area. In place three and four follow the large tropical regions, Africa and S-America with 16.4 (IQR: 14.4–18.3) and 14.2 (IQR: 13.7–15.1) Tg CH<sub>4</sub> yr<sup>-1</sup>, respectively. Together, these four regions are responsible for about three quarters of the global inland water CH<sub>4</sub> emissions estimated here.

Several studies have highlighted the importance of northern lakes in the global methane budget and their potential sensitivity to climate change (Wik et al., 2016). Lake-based methane emissions from N-America and Russia sum to a median emission of 40.2 (range: 19.9–88.4) Tg CH<sub>4</sub> yr<sup>-1</sup> (Table S3 in Supporting Information S2), that is, roughly about 2/3 of global lake CH<sub>4</sub> emissions. For comparison, Wik et al., 2016 estimate that northern lakes and ponds above 50°N emit 16.5 Tg CH<sub>4</sub> yr<sup>-1</sup> (Wik et al., 2016). This estimate would be in line with our regional fluxes given that about 47% of our ice-corrected lake surface area in N-America, Europe and Russia is above 50° latitude. A recent data set increases the sample size of methane emissions from northern lakes and ponds but this information has not yet been upscaled (Kuhn et al., 2021).

The ice correction applied here, which incorporates both winter ice cover and additional methane flux during ice off, resulted in a reduction of global inland water CH<sub>4</sub> emission by 20%. Global lake CH<sub>4</sub> emissions are reduced by 23%, while that of rivers and reservoirs are reduced by only 12% and 17%, respectively. The higher reduction for lake emissions can easily be explained by their high abundance in boreal to arctic regions. The regions with the highest ice cover related reductions of inland water CH<sub>4</sub> emissions are North America (33%) and Russia (26%), where lakes dominate inland water emissions (Table S3 in Supporting Information S2).

## 5. Inland Water N<sub>2</sub>O Budget

For the regionalized area-normalized reassessment of N<sub>2</sub>O emissions from rivers, we only retained the three most recent studies reviewed by Lauerwald et al. (2023a), which provided spatially resolved estimates (Maavara et al., 2019; Marzadri et al., 2021; Yao et al., 2020, see Table S1), see our companion paper for a justification of this choice. For the regionalized reassessment of N<sub>2</sub>O emission from lakes, we distinguished again three types

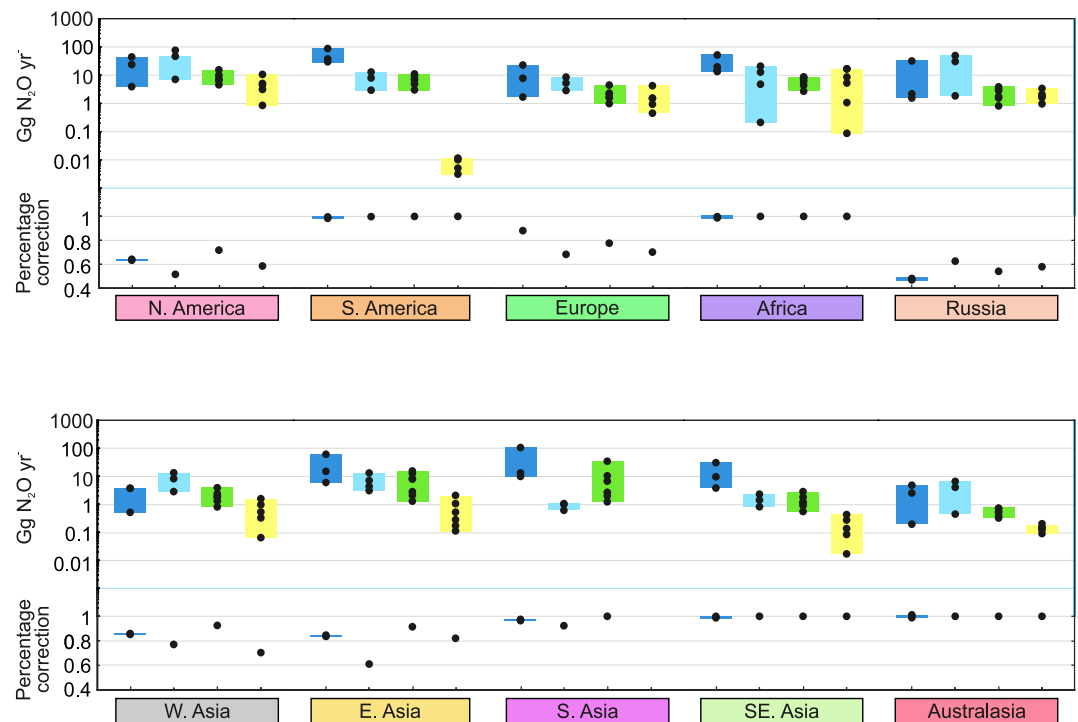
of lakes from the HydroLAKES database: natural lakes, reservoirs, and lakes regulated by dams. Only two estimates reported in Lauerwald et al. (2023a) allowed to distinguish the contribution of all three lake types: the model-based study by Lauerwald et al. (2019) and the direct upscaling approach after DelSontro et al. (2018). For the latter, we applied the average areal emission rate of  $78.6 \text{ mg N}_2\text{O m}^2 \text{ yr}^{-1}$  (DelSontro et al., 2018). Note that this emission rate was derived without separating lakes from reservoirs, and that we used this rate indistinctly to re-estimate the  $\text{N}_2\text{O}$  emissions from the three different types of lakes (natural lakes, reservoirs, lakes with dams). Lauerwald et al. (2019), on the contrary, explicitly made spatially resolved estimates for each of the three types of lakes distinguished here. For reservoirs only, we also included the estimate based on direct upscaling from a global average  $\text{N}_2\text{O}$  emission rate of  $172 \text{ mg N}_2\text{O/m}^2/\text{yr}$  reported by Deemer et al. (2016). This value was derived from observations from this specific water body type, and is about twice as high as the one after DelSontro et al. (2018). Further, we included the model-based studies by Maavara et al. (2019) and Yao et al. (2020) which give area-integrated estimates for dammed water bodies, including both reservoirs (lake types 2) and lakes regulated by a dam (lake type 3). In both cases, we used the area ratio between these two lake types to break down the merged estimates.

Finally, we added three regional estimates in our analysis: the studies by Borges et al. (2015) and Borges et al. (2022) that give estimates for African rivers and lakes, respectively, and the study by Li et al. (2018) that gives estimates for lakes and reservoirs in China. In the latter case, we extrapolated the average flux rates over the whole of RECCAP-2 region 7 (East Asia), which besides China further includes the two Koreas and Japan. The estimates after Borges et al. (2015) are quite comparable to the estimates after Maavara et al. (2019) and Marzadri et al. (2021) for African rivers (Table S1). Note that also Borges et al. (2019) found good agreement between their detailed assessment of  $\text{N}_2\text{O}$  emissions from the Congo River network and the estimates from Maavara et al. (2019). Borges et al. (2022), however, report much lower  $\text{N}_2\text{O}$  emissions from African lakes than derived here from any of the global estimates. They even found that many large lakes in Africa are rather sinks for atmospheric  $\text{N}_2\text{O}$  (Borges et al., 2022). For E-Asian standing waters, estimates after Li et al. (2018) fall in the range of the broken down global estimates for reservoirs and lakes with a dam, but are substantially higher for lakes without a dam.

Our synthesis in Figure 4 shows the range of estimates per RECCAP-2 region, homogenized with regard to inland water surface area and effects of seasonal ice-cover (see Section 2). More detailed results from the statistical analysis of the rescaled emission estimates can be found in Table S4 in Supporting Information S2 and are discussed below. We see that after omitting the older, much higher estimates based on EF approaches (see Lauerwald et al., 2023a), the spread in the estimates of inland water  $\text{N}_2\text{O}$  emissions is substantially reduced (Table S1), but even the retained, area-normalized estimates of inland water  $\text{N}_2\text{O}$  emissions still range over one order of magnitude. At global scale, the surface-area homogenized median (min-max) estimates for aquatic  $\text{N}_2\text{O}$  evasion are  $130 (71\text{--}445) \text{ Gg N}_2\text{O yr}^{-1}$  for streams and rivers,  $120 (23\text{--}205) \text{ Gg N}_2\text{O yr}^{-1}$  for lakes and  $41 (16\text{--}101) \text{ Gg N}_2\text{O yr}^{-1}$  for reservoirs, respectively. Lakes regulated by dams as a third lake type contribute another  $16 (3\text{--}40) \text{ Gg N}_2\text{O yr}^{-1}$ . If we calculate median values (and interquartile ranges - IQR) of all possible combinations per RECCAP-2 region and sum those up (as performed for  $\text{CO}_2$  and  $\text{CH}_4$ ), we obtain a global inland water  $\text{N}_2\text{O}$  evasion flux estimate of  $322 (\text{IQR: } 248\text{--}590) \text{ Gg N}_2\text{O yr}^{-1}$ . This estimate is at the far lower end of the  $500\text{--}1,100 \text{ Gg N}_2\text{O yr}^{-1}$  given in AR6 of the IPCC. Our median global emission flux includes a reduction of 29% due to seasonal ice cover. Despite a surface area of only 1/5 that of global standing water bodies, streams and rivers are the largest contributor to inland water emissions (40%), followed closely by lakes which contribute another 38% of the total aquatic evasion. The most important contributors to global inland water  $\text{N}_2\text{O}$  emissions are N-America, S-America, and Africa, with median emissions of  $83 (\text{IQR: } 59\text{--}108)$ ,  $53 (\text{IQR: } 47\text{--}98)$ , and  $43 (\text{IQR: } 34\text{--}58) \text{ Gg N}_2\text{O yr}^{-1}$ , respectively. These three RECCAP-2 regions account for more than half of the global inland water  $\text{N}_2\text{O}$  emissions.

## 6. Overall Inland Water GHG Budget

To compare estimates of inland water GHG emissions across different gas types, emissions were expressed as  $\text{CO}_2$  equivalents. Using the emission conversion factors recommended by the IPCC AR6, we have calculated the  $\text{CO}_2$  equivalents for a 20 year and 100 years horizon. At the 100 years horizon, 1 kg of  $\text{CH}_4$  or  $\text{N}_2\text{O}$  have the same global warming potential ( $\text{GWP}_{100}$ ) as 27 or 273 kg  $\text{CO}_2$ , respectively. At the 20 years horizon, which is more relevant for projections until the middle of this century, the global warming potential ( $\text{GWP}_{20}$ ) of 1 kg of



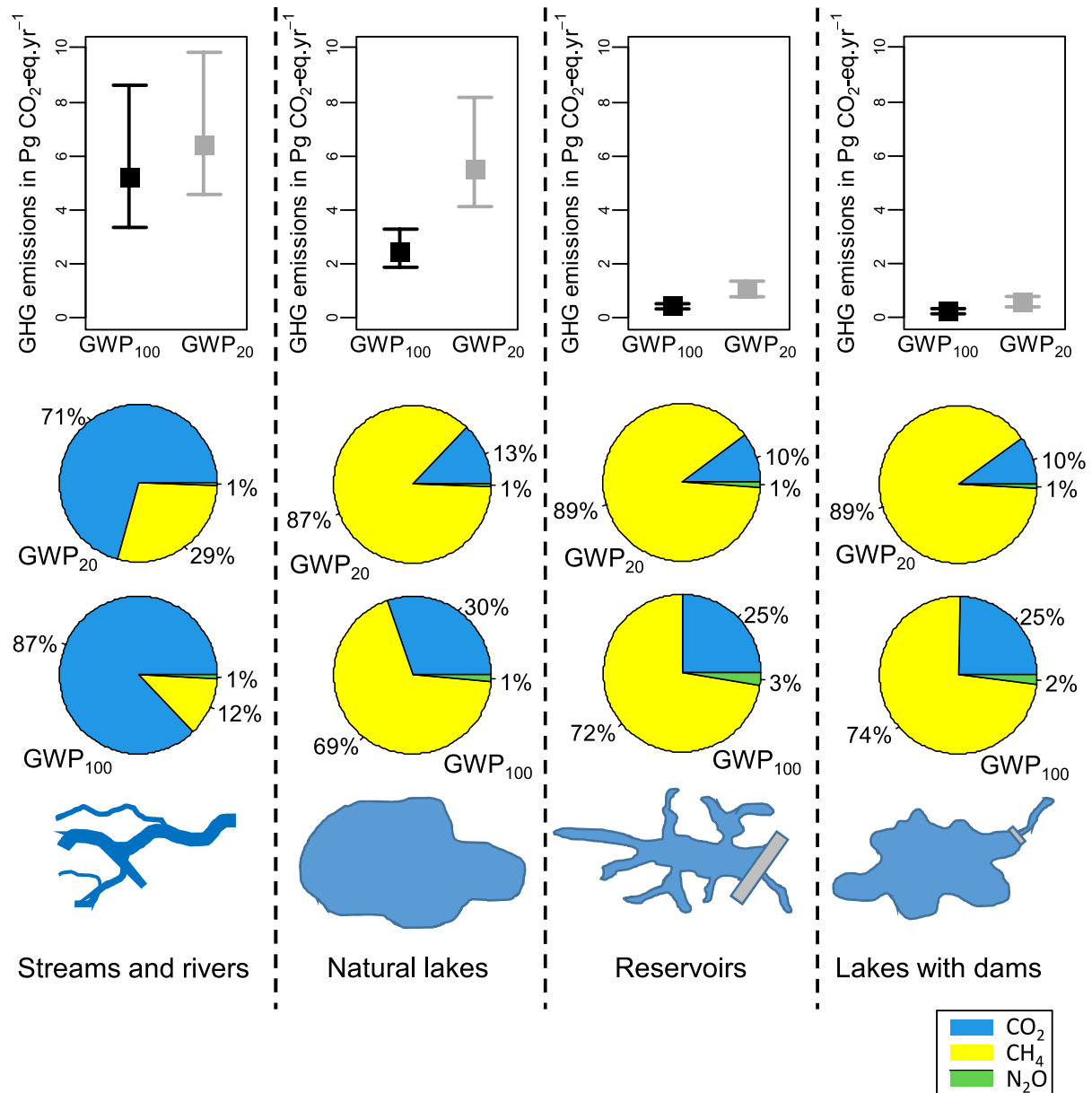
**Figure 4.** Spatial and statistical distribution of standardized inland water  $N_2O$  emission flux. Regional estimates of  $N_2O$  emission ( $Gg N_2O yr^{-1}$ ) in the top bars, ice-corrected surface area estimates in blue lines, and the percent change in total annual emission from the combination of ice and ice melt corrections in the bottom bars. Regional emissions are shown from rivers (dark blue), natural lakes (light blue), reservoirs (green) and lakes with a dam (yellow). Each black dot represents the regionalized emission from one study in the literature, such that the bars show the range of regionalized emissions across studies. More details on the individual values can be found in Table S1.

$CH_4$  reaches that of  $80 kg CO_2$ . This difference is due to the half-life time of  $CH_4$  of 9.1 years. On the other hand, partly due to its long half-life (114 years), the  $N_2O$  warming potential at the 20 years horizon is not different from that at the 100 years horizon.

Further, when combining the estimates for different GHGs and different types of inland waters, a large number of alternative combinations of individual estimates are again possible. First, we simply combined median flux estimates per GHG, inland water type and RECCAP-2 region, which were then summed up to obtain a best estimate of global fluxes. We then added the IQR from all possible combinations of emission estimates per type of inland water, GHG and RECCAP-2 region as bounds to these median estimates. This yielded global inland water emissions with a  $GWP_{20}$  and  $GWP_{100}$  of 13.5 (9.9–20.1) and 8.3 (5.7–12.7)  $Pg CO_2$ -eq.  $yr^{-1}$ , respectively (Figure 5, Table 1).

Considering median estimates, rivers are responsible for more than half (63%) of the  $GWP_{100}$  of global inland water GHG emissions, with a dominant contribution from  $CO_2$  (87%) and a minor contribution from  $CH_4$  (12%) (Figure 5, Table 1). About one third (29%) of total emissions can be attributed to natural lakes (LT1), with minor contributions from reservoirs (LT2, 5%) and lakes regulated by dams (LT3, 3%). In contrast to rivers, for each of the three lake types,  $CH_4$  accounts for more than two thirds of the  $GWP_{100}$ , corroborating earlier global scale assessments by Deemer et al. (2016) and DelSontro et al. (2018). At a 20 years horizon, the contributions of  $CH_4$  emissions are substantially higher as a result of the higher conversion factor. It even becomes the dominant contributor to  $GWP_{20}$  before  $CO_2$  with 59% versus 40%, respectively, while it contributes only 33% to  $GWP_{100}$  (Table 1). Due to the higher weight of  $CH_4$  emissions in  $GWP_{20}$ , lakes are a similarly important contributor to  $GWP_{20}$  compared to rivers. Most surprisingly, the contribution of inland water  $N_2O$  emissions is negligible at both time horizons, in line with previous findings from regional budgets for African inland waters (Borges et al., 2015, 2022) and from a global assessment of reservoir emissions alone (Deemer et al., 2016).

Figure 6 shows the statistical distribution of the rescaled estimates for each of the three GHGs and the 10 RECCAP-2 regions. The most important regional contributors to the  $GWP_{20}$  and  $GWP_{100}$  of global inland water



**Figure 5.** Global Warming Potential (GWP) (GWP) of inland water greenhouse gas emissions at 20 (GWP<sub>20</sub>) and 100 (GWP<sub>100</sub>) year horizon based on rescaled estimates (medians and interquartile ranges of all possible combinations), distinguishing contributions from rivers and three types of lakes: natural lakes, reservoirs and lakes regulated by dams. Relative contributions of CO<sub>2</sub>, CH<sub>4</sub> and N<sub>2</sub>O to GWP<sub>20</sub> and GWP<sub>100</sub> are based on medians of estimates.

GHG emissions are N- and S-America, followed by Russia and Africa (Table 1). These four regions together contribute about three quarters to the GWPs of global inland water emissions. That ranking is however heavily influenced by the areal extent of each RECCAP-2 region. If we normalize emissions by the area of RECCAP-2 regions, we identify the highest CO<sub>2</sub>-equivalent emission rates for SE-Asia, followed by S-America and Russia (Table 1). Rivers are the dominant contributors to GWPs of inland water emissions in S-America and SE-Asia, while in N-America and Russia lakes have a much higher weight.

From the range of estimates reported in Figure 6, we see once again that inland water N<sub>2</sub>O emissions are the least well constrained. However, based on the ensemble of estimates, the contribution of N<sub>2</sub>O to the GWP of inland water GHG emissions seems to be negligible in most areas of the world. CO<sub>2</sub> is the largest contributor to the GWP<sub>100</sub> of inland water GHG emissions in S-America, S-, E- and SE-Asia. On the contrary, contributions

**Table 1**  
Global Warming Potential at 20 (GWP<sub>20</sub>) and 100 (GWP<sub>100</sub>) Year Horizons

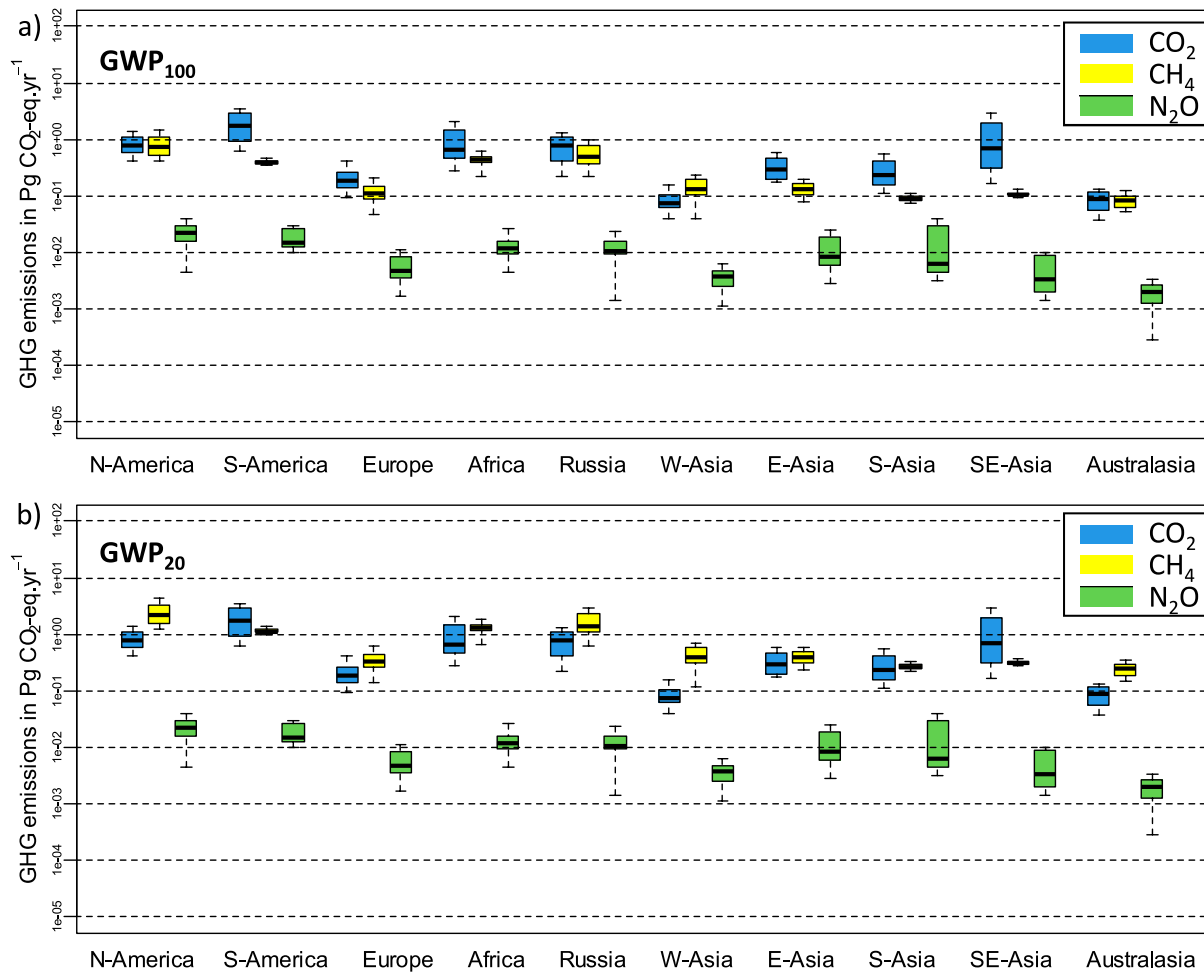
GWP20										
RECCAP2 zone		Total emissions (median [IQ range])		Contribution per gas [%]			Contribution per inland water type [%]			
No	Name	Tg CO <sub>2-eq</sub> /yr	g CO <sub>2-eq</sub> /m <sup>2</sup> /yr*	CO <sub>2</sub>	CH <sub>4</sub>	N <sub>2</sub> O	Rivers**	LT1**	LT2**	LT3**
1	N-America	2,842 (2,109–4,495)	117 (87–185)	25	74	1	16	71	8	5
2	S-America	2,855 (2,142–3,793)	160 (120–212)	60	40	1	80	13	7	0
3	Europe	525 (409–725)	88 (69–122)	33	66	1	33	47	12	8
4	Africa	2,041 (1,575–2,991)	68 (52–99)	32	67	1	48	30	9	13
5	Russia	2,223 (1,492–3,519)	132 (88–208)	34	65	0	33	58	5	4
6	W-Asia	469 (357–686)	44 (33–64)	15	84	1	11	76	10	3
7	E-Asia	701 (475–990)	60 (41–85)	43	56	1	51	36	11	1
8	S-Asia	515 (400–689)	115 (90–154)	47	52	1	76	8	16	0
9	SE-Asia	1,017 (681–1,794)	201 (135–355)	69	31	0	87	9	4	1
10	Australia	340 (235–414)	43 (29–52)	24	75	1	27	66	6	2
	Global	13,528 (9,875–20,097)	100 (73–149)	40	59	1	47	41	8	4
GWP100										
RECCAP2 zone		Total emissions (median [IQ range])		Contribution per gas [%]			Contribution per inland water type [%]			
No	Name	Tg CO <sub>2-eq</sub> /yr	g CO <sub>2-eq</sub> /m <sup>2</sup> /yr*	CO <sub>2</sub>	CH <sub>4</sub>	N <sub>2</sub> O	Rivers**	LT1**	LT2**	LT3**
1	N-America	1,445 (1,164–2,174)	60 (48–90)	49	50	2	26	63	7	4
2	S-America	2,108 (1,406–2,994)	118 (79–168)	81	18	1	88	8	4	0
3	Europe	313 (226–417)	53 (38–70)	59	40	2	47	38	8	7
4	Africa	1,127 (828–2,033)	37 (28–68)	58	41	1	64	21	7	9
5	Russia	1,304 (785–1,901)	77 (46–113)	61	39	1	48	45	4	3
6	W-Asia	211 (169–289)	20 (16–27)	34	64	2	19	69	9	3
7	E-Asia	442 (303–650)	38 (26–56)	68	30	2	67	24	8	1
8	S-Asia	343 (252–483)	77 (56–108)	71	27	2	84	5	10	0
9	SE-Asia	808 (484–1,577)	160 (96–312)	86	13	0	93	5	2	0
10	Australia	169 (124–216)	21 (16–27)	48	51	1	44	51	5	1
	Global	8,269 (5,741–12,735)	61 (43–94)	66	33	1	63	29	5	3

*Note.* Emissions are given as the median (interquartile range) of CO<sub>2</sub> equivalents. Relative contribution per gas and inland water type refer to median estimates. \*global warming potential of inland water emissions expressed as rates of CO<sub>2</sub> equivalents normalized by the total area (terrestrial + wetland + inland water) of each RECCAP-2 region. \*\*Inland water types considered in this study: Rivers (all flowing waters including from small headwater streams to large rivers) and three lake types (LT)–LT1 = natural lakes, LT2 = reservoirs, LT3 = lakes regulated by a dam.

of CH<sub>4</sub> to GWP<sub>100</sub> of inland water emissions are higher than that of CO<sub>2</sub> in N-America, W-Asia, and Australasia (Table 1). The relative contribution of CH<sub>4</sub> is clearly linked to the contribution of lakes to the inland water emissions (Table 1), for which the proportion of CH<sub>4</sub> in the overall GWPs is much higher than for rivers (Figure 5). For GWP<sub>20</sub>, for which the relative weight of CH<sub>4</sub> is stronger, CH<sub>4</sub> appears to be the most important contributor for eight of the 10 RECCAP-2 regions (Table 1). The two exceptions, S-America and SE-Asia, are strongly dominated by emissions from rivers and thus also by emissions of CO<sub>2</sub>.

## 7. Conclusions and Outlook

From our synthesis of inland water GHG emission estimates, we obtained estimates of global CO<sub>2</sub> emissions of 5.5 (IQR: 3.5–9.1) Pg CO<sub>2</sub> yr<sup>-1</sup>, which are comparable to the values obtained in RECCAP-1 (Raymond et al., 2013). In contrast, our synthesized global estimates for CH<sub>4</sub> (100, IQR: 82–135 Tg CH<sub>4</sub> yr<sup>-1</sup>) and N<sub>2</sub>O (322, IQR: 248–590 Gg N<sub>2</sub>O yr<sup>-1</sup>) emissions fall on the lower end of the range of estimates reported in AR6 of the IPCC.



**Figure 6.** Spatial and statistical distribution of Global Warming Potentials of standardized inland water GHG emissions. Regional estimates of  $\text{CO}_2$ ,  $\text{CH}_4$ , and  $\text{N}_2\text{O}$ , expressed as  $\text{CO}_2$  equivalents at (a) 100 years and (b) 20 years horizon. The boxplots represent median, interquartile range and total range of rescaled estimates per RECCAP-2 region.

We find remarkable differences in the contributions of rivers, lakes, and reservoirs, and of the 10 RECCAP-2 regions to global inland water GHG emissions. South-American rivers contribute about one third of global inland water  $\text{CO}_2$  emissions. North-American and Russian lakes contribute together one third of global inland water  $\text{CH}_4$  emissions. And finally, North America alone contributes one fourth of global inland water  $\text{N}_2\text{O}$  emissions.

Our synthesis suggests that global inland water GHG emissions have a GWP of 8.3 (IQR: 5.7–12.7) or 13.5 (IQR: 9.9–20.1)  $\text{Pg CO}_2\text{-eq. yr}^{-1}$  at a 100 or 20 years horizon, respectively. In terms of GWP, inland water emissions of  $\text{CO}_2$  and  $\text{CH}_4$  are of similar importance, with  $\text{CO}_2$  dominating emissions from rivers and  $\text{CH}_4$  dominating emissions from lakes, while contributions from  $\text{N}_2\text{O}$  seem by far less important for any type of inland waters. In addition, inland water emissions have different importance for the overall continental budgets of  $\text{CO}_2$ ,  $\text{CH}_4$ , and  $\text{N}_2\text{O}$ . While inland water  $\text{N}_2\text{O}$  emissions already appear rather small compared to emissions of  $\text{CO}_2$  and  $\text{CH}_4$ , their contribution to the global  $\text{N}_2\text{O}$  budget appears also negligible. Our synthesized estimate does not represent more than 1% of global emission of 53  $\text{Tg N}_2\text{O yr}^{-1}$  synthesized in the first global  $\text{N}_2\text{O}$  budget of the Global Carbon Project (GCP) (Tian et al., 2020). But also inland water  $\text{CO}_2$  emissions, which are important in terms of GWP and total flux in the overall GHG budget of inland waters, are relatively small compared to other flux components of the continental  $\text{CO}_2$  budget. Being mostly fed by autotrophic and heterotrophic respiration in upland soils, wetlands and aquatic systems (Abril & Borges, 2019; Battin et al., 2023), it is fair to consider inland water  $\text{CO}_2$  emissions as a fraction of continental ecosystem respiration. Our synthesized estimate of global inland water  $\text{CO}_2$  emissions would represent only about 1%–2% of continental ecosystem respiration (cf. Battin et al., 2023;

Ciais et al., 2021), a proportion much lower than the uncertainties related to the quantification of this flux at global scale. However, inland water emissions are in the order of magnitude of net- $\text{CO}_2$  uptake by terrestrial ecosystems (land C sink minus LUC emissions, Friedlingstein et al., 2020), and should thus be represented in detailed  $\text{CO}_2$  budgets. Dynamic global vegetation models simulate  $\text{CO}_2$  budgets of continental ecosystems while ignoring aquatic C cycling (Ciais et al., 2021). However, those models may simply compensate for this missing flux of inland water  $\text{CO}_2$  emissions by a slightly higher soil respired  $\text{CO}_2$  emission flux, while biases in simulated land  $\text{CO}_2$  uptake may rather be linked to the non-representation of lateral C exports to the coast (Lauerwald et al., 2020). Also, global scale atmospheric inversions usually do not consider inland waters as a specific source of emissions, because it is not possible to separate terrestrial and aquatic signals due to the coarse resolution of inversions and the relatively small size of most inland waters. In contrast, estimates of terrestrial  $\text{CO}_2$  budgets upscaled from flux tower measurements (e.g., FLUXCOM, Jung et al., 2020), which focus more explicitly on terrestrial ecosystems or wetlands, will not account for inland water emissions, and would need to be complemented with corresponding estimates.

In contrast to  $\text{CO}_2$  and  $\text{N}_2\text{O}$ , global inland water  $\text{CH}_4$  emissions could easily represent  $\sim 20\%$  of global total emissions of  $576 \text{ Tg CH}_4 \text{ yr}^{-1}$  estimated from atmospheric inversion in the most recent global methane budget by Saunio et al. (2020). The potential importance of inland water  $\text{CH}_4$  emissions is even higher if compared to the top-down estimate of only natural emissions of  $218 \text{ Tg CH}_4 \text{ yr}^{-1}$  (Saunio et al., 2020). In the global methane budget of the GCP, inland water  $\text{CH}_4$  emissions are grouped into the category “other natural emissions,” together with emissions from geologic sources, termites, vegetation, oceans, wild animals and permafrost. This category complements “wetlands” as a major natural source of  $\text{CH}_4$ . Interestingly, bottom-up estimates of these “other natural emissions” are much higher than the corresponding estimates based on atmospheric inversions, with  $222 (143\text{--}306) \text{ Tg CH}_4 \text{ yr}^{-1}$  versus  $37 (21\text{--}50) \text{ Tg CH}_4 \text{ yr}^{-1}$  (mean and range, Saunio et al., 2020). Thus, the estimates from our synthesis seem rather high if compared to this top-down estimate. In contrast to this, in the same budget, bottom-up estimates tend to be lower than top-down estimates for “wetland emissions” with  $149 (102\text{--}182)$  versus  $182 (159\text{--}200) \text{ Tg CH}_4 \text{ yr}^{-1}$  (mean and range, Saunio et al., 2020). As wetlands and inland waters may be spatially correlated at regional to global scales, it is difficult to distinguish both sources in inversions. Thus, it may be possible that wetlands as methane source may have been overestimated to the detriment of inland water sources. More systematic investigations of  $\text{CH}_4$  emissions from upland, wetland and aquatic ecosystems will be needed to clarify what causes the mismatch between top-down and bottom up estimates, and to more accurately separate wetland from aquatic emissions of  $\text{CH}_4$ .

One of the greatest weaknesses of our synthesis is the non-representation of smallest standing water bodies with an area  $< 0.1 \text{ km}^2$  and which may contribute substantially to  $\text{CH}_4$  and  $\text{CO}_2$  emissions (Holgerson & Raymond, 2016). The order of magnitude of the contribution of these smallest water bodies to global inland water emissions is however disputed, as the area of these systems can only be guessed. Holgerson and Raymond (2016), for instance, used estimates from Downing et al. (2006) who had established a power-law relationship between lake size and frequency for lakes  $> 10 \text{ km}^2$  taken from global inventories, which they then extrapolated to smaller water bodies down to systems as small as  $0.001 \text{ km}^2$ . This approach has however received criticism and empirical prove has been provided that such power-law distribution does indeed not hold true for small lakes and ponds (Cael & Seekell, 2016). In addition, more data on emission rates, including  $\text{CH}_4$  ebullition, are required. Our estimates of total inland water GHG emissions are thus still likely conservative. Future estimates should try to include these smaller water bodies, which may make separation between wetland and aquatic systems further challenging. Along the same lines, there are certain types of small wetlands, like fringing lacustrine and riverine wetlands, which are not included in this study, and which are not yet included in any global wetland GHG assessment. Same is true for ephemeral water bodies, which are also not included in our synthesis. However, progress is being made in mapping periodic drying of inland waters (Messenger et al., 2021), and data are being collected showing the potential importance of emissions from dry fallen and rewetted bed sediments (Keller et al., 2021). Future assessments of inland water GHG emission may thus include these emissions. While this synthesis effort presented here is an important step forward in including inland waters in regionalised GHG budgets, future research has to invest more efforts into the consistent integration of GHG budgets of inland water, wetland and terrestrial ecosystems.

### Data Availability Statement

The data that support the findings of this study are available at figshare: Lauerwald et al. (2023b) (<https://doi.org/10.6084/m9.figshare.22492504>).

**Acknowledgments**

Any use of trade, firm, or product names is for descriptive purposes only and does not imply endorsement by the US Government. Ronny Lauerwald acknowledges funding from French state aid, managed by ANR under the “Investissements d’avenir” programme (ANR-16-CONV-0003), and from the European Union’s Horizon Europe Research and Innovation programme under Grant Agreement No. 101060423. George Allen was funded by a US National Science Foundation CAREER Award (Grant EAR 2145628). Shaoda Liu was funded by the National Key Research and Development Program of China (2021YFC3200401). Matthew Johnson was funded for this work by NASA’s Interdisciplinary Research in Earth Science (IDS) Program and the NASA Terrestrial Ecology and Tropospheric Composition Programs. Adam Hastie was funded by NERC (Grant Ref. NE/R000751/1) and by Charles University (Grant Ref. PRIMUS23/SCI/013). David Bastviken was funded by the European Research Council (ERC; Grant Agreement No. 725546; METLAKE), the Swedish Research Council (Grant 2016-04829), and FORMAS (Grant 2018-01794). Meredith Holgerson was funded by a US National Science Foundation CAREER Award (Grant DEB 2143449). Pierre Regnier acknowledges funding from the European Union’s Horizon 2020 research and innovation program under Grant Agreement No. 101003536 (ESM2025—Earth System Models for the Future) and from the FRS-FRNS PDR project T.0191.23 CH4-lakes. Alessandra Marzadri acknowledges funding from the Italian Ministry of Education, University and Research (MIUR) in the frame of the Departments of Excellence Initiative 2023–2027 and from the project iNEST—Interconnected Nord-Est Innovation Ecosystem (ECS00000043 – CUP E63C22001030007). Lishan Ran was funded by the Research Grants Council of Hong Kong (Grant 17300621). Hanqin Tian acknowledges funding from US National Science Foundation award (Grant 1903722). Taylor Maavara and Lewis Alcott were funded by the Hutchinson Fellowship Program from the Yale Institute of Biospheric Studies at Yale University.

**References**

Abril, G., & Borges, A. V. (2019). Ideas and perspectives: Carbon leaks from flooded land: Do we need to replumb the inland water active pipe? *Biogeosciences*, *16*(3), 769–784. <https://doi.org/10.5194/bg-16-769-2019>

Abril, G., Bouillon, S., Darchambeau, F., Teodoru, C. R., Marwick, T. R., Tamooh, F., et al. (2015). Technical Note: Large overestimation of pCO<sub>2</sub> calculated from pH and alkalinity in acidic, organic-rich freshwaters. *Biogeosciences*, *12*(1), 67–78. <https://doi.org/10.5194/bg-12-67-2015>

Allen, G. H., & Pavelsky, T. (2018). Global extent of rivers and streams. *Science*, *361*(6402), 585–588. <https://doi.org/10.1126/science.aat063>

Allen, P. M., Arnold, J. C., & Byars, B. W. (1994). Downstream channel geometry for use in planning-level models. *JAWRA Journal of the American Water Resources Association*, *30*(4), 663–671. <https://doi.org/10.1111/j.1752-1688.1994.tb03321.x>

Aufdenkampe, A. K., Mayorga, E., Raymond, P. A., Melack, J. M., Doney, S. C., Alin, S. R., et al. (2011). Riverine coupling of biogeochemical cycles between land, oceans, and atmosphere. *Frontiers in Ecology and the Environment*, *9*(1), 53–60. <https://doi.org/10.1890/100014>

Bastos, A., O’Sullivan, M., Ciais, P., Makowski, D., Sitch, S., Friedlingstein, P., et al. (2020). Sources of uncertainty in regional and global terrestrial CO<sub>2</sub> exchange estimates. *Global Biogeochemical Cycles*, *34*(2), e2019GB006393. <https://doi.org/10.1029/2019GB006393>

Bastviken, D., Tranvik, L. J., Downing, J. A., Crill, P. M., & Enrich-Prast, A. (2011). Freshwater methane emissions offset the continental carbon sink. *Science*, *331*(6013), 50. <https://doi.org/10.1126/science.1196808>

Battin, T. J., Lauerwald, R., Bernhardt, E. S., Bertuzzo, E., Gener, L. G., Hall, R. O., et al. (2023). River ecosystem metabolism and carbon biogeochemistry in a changing world. *Nature*, *613*(7944), 449–459. <https://doi.org/10.1038/s41586-022-05500-8>

Borges, A. V., Darchambeau, F., Lambert, T., Morana, C., Allen, G. H., Tambwe, E., et al. (2019). Variations in dissolved greenhouse gases (δ chemCO<sub>2</sub>, δ chemCH<sub>4</sub>, δ chemN<sub>2</sub>O) in the Congo River network overwhelmingly driven by fluvial-wetland connectivity. *Biogeosciences*, *16*(19), 3801–3834. <https://doi.org/10.5194/bg-16-3801-2019>

Borges, A. V., Darchambeau, F., Teodoru, C. R., Marwick, T. R., Tamooh, F., Geeraert, N., et al. (2015). Globally significant greenhouse-gas emissions from African inland waters. *Nature Geoscience*, *8*(8), 637–642. <https://doi.org/10.1038/ngeo2486>

Borges, A. V., Deirmendjian, L., Bouillon, S., Okello, W., Lambert, T., Roland, F. A. E., et al. (2022). Greenhouse gas emissions from African lakes are No longer a blind spot. *Science Advances*, *8*(25), eabi8716. <https://doi.org/10.1126/sciadv.abi8716>

Butman, D., & Raymond, P. A. (2011). Significant efflux of carbon dioxide from streams and rivers in the United States. *Nature Geoscience*, *4*(12), 839–842. <https://doi.org/10.1038/ngeo1294>

Cael, B., & Seekell, D. (2016). The size-distribution of Earth’s lakes. *Scientific Reports*, *6*(1), 29633. <https://doi.org/10.1038/srep29633>

Cavaliere, E., & Baulch, H. M. (2018). Denitrification under lake ice. *Biogeochemistry*, *137*(3), 285–295. <https://doi.org/10.1007/s10533-018-0419-0>

Ciais, P., Bastos, A., Chevallier, F., Lauerwald, R., Poulter, B., Canadell, P., et al. (2022). Definitions and methods to estimate regional land carbon fluxes for the second phase of the REgional Carbon Cycle Assessment and Processes Project (RECCAP-2). *Geoscientific Model Development*, *15*(3), 1289–1316. <https://doi.org/10.5194/gmd-15-1289-2022>

Ciais, P., Yao, Y., Gasser, T., Baccini, A., Wang, Y., Lauerwald, R., et al. (2021). Empirical estimates of regional carbon budgets imply reduced global soil heterotrophic respiration. *National Science Review*, *8*(2). <https://doi.org/10.1093/nsr/nwaa145>

Cole, J. J., Prairie, Y. T., Caraco, N. F., McDowell, W. H., Tranvik, L. J., Striegl, R. G., et al. (2007). Plumbing the global carbon Cycle: Integrating inland waters into the terrestrial carbon budget. *Ecosystems*, *10*(1), 172–185. <https://doi.org/10.1007/s10021-006-9013-8>

Deemer, B. R., Harrison, J. A., Li, S., Beaulieu, J. J., DelSontro, T., Barros, N., et al. (2016). Greenhouse gas emissions from reservoir water surfaces: A new global synthesis. *BioScience*, *66*(11), 949–964. <https://doi.org/10.1093/biosci/biw117>

DelSontro, T., Beaulieu, J. J., & Downing, J. A. (2018). Greenhouse gas emissions from lakes and impoundments: Upscaling in the face of global change. *Limnology and Oceanography Letters*, *3*(3), 64–75. <https://doi.org/10.1002/lo.120073>

Denfeld, B. A., Baulch, H. M., del Giorgio, P. A., Hampton, S. E., & Karlsson, J. (2018). A synthesis of carbon dioxide and methane dynamics during the ice-covered period of northern lakes. *Limnology and Oceanography Letters*, *3*(3), 117–131. <https://doi.org/10.1002/lo.120079>

Downing, J. A., Prairie, Y. T., Cole, J. J., Duarte, C. M., Tranvik, L. J., Striegl, R. G., et al. (2006). The global abundance and size distribution of lakes, ponds, and impoundments. *Limnology & Oceanography*, *51*(5), 2388–2397. <https://doi.org/10.4319/lo.2006.51.5.2388>

Fick, S. E., & Hijmans, R. J. (2017). WorldClim 2: New 1-km spatial resolution climate surfaces for global land areas. *International Journal of Climatology*, *37*(12), 4302–4315. <https://doi.org/10.1002/joc.5086>

Friedlingstein, P., O’Sullivan, M., Jones, M. W., Andrew, R. M., Hauck, J., Olsen, A., et al. (2020). Global carbon budget 2020. *Earth System Science Data*, *12*(4), 3269–3340. <https://doi.org/10.5194/essd-12-3269-2020>

Harrison, J. A., Prairie, Y. T., Mercier-Blais, S., & Soued, C. (2021). Year-2020 global distribution and pathways of reservoir methane and carbon dioxide emissions according to the greenhouse gas from reservoirs (G-res) model. *Global Biogeochemical Cycles*, *35*(6), e2020GB006888. <https://doi.org/10.1029/2020GB006888>

Hastie, A., Lauerwald, R., Weyhenmeyer, G., Sobek, S., Verpoorter, C., & Regnier, P. (2018). CO<sub>2</sub> evasion from boreal lakes: Revised estimate, drivers of spatial variability, and future projections. *Global Change Biology*, *24*(2), 711–728. <https://doi.org/10.1111/gcb.13902>

Holgerson, M. A., & Raymond, P. A. (2016). Large contribution to inland water CO<sub>2</sub> and CH<sub>4</sub> emissions from very small ponds. *Nature Geoscience*, *9*(3), 222–226. <https://doi.org/10.1038/ngeo2654>

Horghby, Å., Segatto, P. L., Bertuzzo, E., Lauerwald, R., Lehner, B., Ulseth, A. J., et al. (2019). Unexpected large evasion fluxes of carbon dioxide from turbulent streams draining the world’s mountains. *Nature Communications*, *10*(1), 4888. <https://doi.org/10.1038/s41467-019-12905-z>

Hu, M., Chen, D., & Dahlgren, R. A. (2016). Modeling nitrous oxide emission from rivers: A global assessment. *Global Change Biology*, *22*(11), 3566–3582. <https://doi.org/10.1111/gcb.13351>

Johnson, M. S., Matthews, E., Bastviken, D., Deemer, B., Du, J., & Genovese, V. (2021). Spatiotemporal methane emission from global reservoirs. *Journal of Geophysical Research: Biogeosciences*, *126*(8), e2021JG006305. <https://doi.org/10.1029/2021JG006305>

Johnson, M. S., Matthews, E., Du, J., Genovese, V., & Bastviken, D. (2022). Methane emission from global lakes: New spatiotemporal data and observation-driven modeling of methane dynamics indicates lower emissions. *Journal of Geophysical Research: Biogeosciences*, *127*(7), e2022JG006793. <https://doi.org/10.1029/2022JG006793>

Jung, M., Schwalm, C., Migliavacca, M., Walther, S., Camps-Valls, G., Koiraal, S., et al. (2020). Scaling carbon fluxes from eddy covariance sites to globe: Synthesis and evaluation of the FLUXCOM approach. *Biogeosciences*, *17*(5), 1343–1365. <https://doi.org/10.5194/bg-17-1343-2020>

Karlsson, J., Serikova, S., Vorobyev, S. N., Rocher-Ros, G., Denfeld, B., & Pokrovsky, O. S. (2021). Carbon emission from Western Siberian inland waters. *Nature Communications*, *12*(1), 825. <https://doi.org/10.1038/s41467-021-21054-1>

Keller, P. S., Marcé, R., Obrador, B., & Koschorreck, M. (2021). Global carbon budget of reservoirs is overturned by the quantification of draw-down areas. *Nature Geoscience*, *14*(6), 402–408. <https://doi.org/10.1038/s41561-021-00734-z>

Kuhn, M. A., Varner, R. K., Bastviken, D., Crill, P., MacIntyre, S., Turetsky, M., et al. (2021). BAWLD-CH4: A comprehensive dataset of methane fluxes from boreal and arctic ecosystems. *Earth System Science Data*, *13*(11), 5151–5189. <https://doi.org/10.5194/essd-13-5151-2021>

- Lauerwald, R., Allen, G. H., Deemer, B. R., Liu, S., Maavara, T., Raymond, P., et al. (2023a). Inland water greenhouse gas budgets for RECCAP-2: 1. State-of-the-Art of global scale assessments. *Global Biogeochemical Cycles*, *37*, e2022GB007657. <https://doi.org/10.1029/2022GB007657>
- Lauerwald, R., Allen, G. H., Deemer, B. R., Liu, S., Maavara, T., Raymond, P., et al. (2023b). Table S1—Rescaled and regionalized inland water greenhouse gas budgets for RECCAP-2. <https://doi.org/10.6084/m9.figshare.22492504>
- Lauerwald, R., Laruelle, G. G., Hartmann, J., Ciais, P., & Regnier, P. A. G. (2015). Spatial patterns in CO<sub>2</sub> evasion from the global river network. *Global Biogeochemical Cycles*, *29*(5), 534–554. <https://doi.org/10.1002/2014GB004941>
- Lauerwald, R., Regnier, P., Camino-Serrano, M., Guenet, B., Guimberteau, M., Ducharne, A., et al. (2017). ORCHILEAK (revision 3875): A new model branch to simulate carbon transfers along the terrestrial-aquatic continuum of the Amazon basin. *Geoscientific Model Development*, *10*(10), 3821–3859. <https://doi.org/10.5194/gmd-10-3821-2017>
- Lauerwald, R., Regnier, P., Figueiredo, V., Enrich-Prast, A., Bastviken, D., Lehner, B., et al. (2019). Natural lakes are a minor global source of N<sub>2</sub>O to the atmosphere. *Global Biogeochemical Cycles*, *33*(12), 1564–1581. <https://doi.org/10.1029/2019GB006261>
- Lauerwald, R., Regnier, P., Guenet, B., Friedlingstein, P., & Ciais, P. (2020). How simulations of the land carbon sink are biased by ignoring fluvial carbon transfers: A case study for the Amazon basin. *One Earth*, *3*(2), 226–236. <https://doi.org/10.1016/j.oneear.2020.07.009>
- Li, S., Bush, R. T., Santos, I. R., Zhang, Q., Song, K., Mao, R., et al. (2018). Large greenhouse gases emissions from China's lakes and reservoirs. *Water Research*, *147*, 13–24. <https://doi.org/10.1016/j.watres.2018.09.053>
- Linke, S., Lehner, B., Ouellet Dallaire, C., Ariwi, J., Grill, G., Anand, M., et al. (2019). Global hydro-environmental sub-basin and river reach characteristics at high spatial resolution. *Scientific Data*, *6*(1), 283. <https://doi.org/10.1038/s41597-019-0300-6>
- Liu, S., Kuhn, C., Amatulli, G., Aho, K., Butman, D. E., Allen, G. H., et al. (2022). The importance of hydrology in routing terrestrial carbon to the atmosphere via global streams and rivers. *Proceedings of the National Academy of Sciences*, *119*(11), e2106322119. <https://doi.org/10.1073/pnas.2106322119>
- Maavara, T., Lauerwald, R., Laruelle, G. G., Akbarzadeh, Z., Bouskell, N. J., Van Cappellen, P., & Regnier, P. (2019). Nitrous oxide emissions from inland waters: Are IPCC estimates too high? *Global Change Biology*, *25*(2), 473–488. <https://doi.org/10.1111/gcb.14504>
- Marzadri, A., Amatulli, G., Tonina, D., Bellin, A., Shen, L. Q., Allen, G. H., & Raymond, P. A. (2021). Global riverine nitrous oxide emissions: The role of small streams and large rivers. *Science of the Total Environment*, *776*, 145148. <https://doi.org/10.1016/j.scitotenv.2021.145148>
- Message, M. L., Lehner, B., Cockburn, C., Lamouroux, N., Pella, H., Snelder, T., et al. (2021). Global prevalence of non-perennial rivers and streams. *Nature*, *594*(7863), 391–397. <https://doi.org/10.1038/s41586-021-03565-5>
- Message, M. L., Lehner, B., Grill, G., Nedeva, I., & Schmitt, O. (2016). Estimating the volume and age of water stored in global lakes using a geo-statistical approach. *Nature Communications*, *7*(1), 13603. <https://doi.org/10.1038/ncomms13603>
- Murfitt, J., & Brown, L. C. (2017). Lake ice and temperature trends for Ontario and Manitoba: 2001 to 2014. *Hydrological Processes*, *31*(21), 3596–3609. <https://doi.org/10.1002/hyp.11295>
- Pi, X., Luo, Q., Feng, L., Xu, Y., Tang, J., Liang, X., et al. (2022). Mapping global lake dynamics reveals the emerging roles of small lakes. *Nature Communications*, *13*(1), 5777. <https://doi.org/10.1038/s41467-022-33239-3>
- Ran, L., Butman, D. E., Battin, T. J., Yang, X., Tian, M., Duvert, C., et al. (2021). Substantial decrease in CO<sub>2</sub> emissions from Chinese inland waters due to global change. *Nature Communications*, *12*(1), 1730. <https://doi.org/10.1038/s41467-021-21926-6>
- Raymond, P. A., Hartmann, J., Lauerwald, R., Sobek, S., McDonald, C., Hoover, M., et al. (2013). Global carbon dioxide emissions from inland waters. *Nature*, *503*(7476), 355–359. <https://doi.org/10.1038/nature12760>
- Rosentreter, J. A., Borges, A. V., Deemer, B. R., Holgerson, M. A., Liu, S., Song, C., et al. (2021). Half of global methane emissions come from highly variable aquatic ecosystem sources. *Nature Geoscience*, *14*(4), 225–230. <https://doi.org/10.1038/s41561-021-00715-2>
- Saunio, M., Stavert, A. R., Poulter, B., Bousquet, P., Canadell, J. G., Jackson, R. B., et al. (2020). The global methane budget 2000–2017. *Earth System Science Data*, *12*(3), 1561–1623. <https://doi.org/10.5194/essd-12-1561-2020>
- Serikova, S., Pokrovsky, O. S., Laudon, H., Krickov, I. V., Lim, A. G., Manasypov, R. M., & Karlsson, J. (2019). High carbon emissions from the tundra lakes of Western Siberia. *Nature Communications*, *10*(1), 1552. <https://doi.org/10.1038/s41467-019-09592-1>
- Sharma, S., Blagrove, K., Magnuson, J. J., O'Reilly, C. M., Oliver, S., Batt, R. D., et al. (2019). Widespread loss of lake ice around the Northern Hemisphere in a warming world. *Nature Climate Change*, *9*(3), 227–231. <https://doi.org/10.1038/s41558-018-0393-5>
- Soued, C., del Giorgio, P. A., & Maranger, R. (2016). Nitrous oxide sinks and emissions in boreal aquatic networks in Québec. *Nature Geoscience*, *9*(2), 116–120. <https://doi.org/10.1038/ngeo2611>
- Stanley, E. H., Casson, N. J., Christel, S. T., Crawford, J. T., Loken, L. C., & Oliver, S. K. (2016). The ecology of methane in streams and rivers: Patterns, controls, and global significance. *Ecological Monographs*, *86*(2), 146–171. <https://doi.org/10.1890/15-1027>
- Stavert, A. R., Saunio, M., Canadell, J. G., Poulter, B., Jackson, R. B., Regnier, P., et al. (2022). Regional trends and drivers of the global methane budget. *Global Change Biology*, *28*(1), 182–200. <https://doi.org/10.1111/gcb.15901>
- St. Louis, V. L., Kelly, C. A., Duchemin, É., Rudd, J. W. M., & Rosenberg, D. M. (2000). Reservoir surfaces as sources of greenhouse gases to the atmosphere: A global estimate: Reservoirs are sources of greenhouse gases to the atmosphere, and their surface areas have increased to the point where they should be included in global inventories of anthropogenic emissions of greenhouse gases. *BioScience*, *50*(9), 766–775. [https://doi.org/10.1641/0006-3568\(2000\)050\[0766:RSASOG\]2.0.CO;2](https://doi.org/10.1641/0006-3568(2000)050[0766:RSASOG]2.0.CO;2)
- Tian, H., Ren, W., Yang, J., Tao, B., Cai, W., Lohrenz, S. E., et al. (2015). Climate extremes dominating seasonal and interannual variations in carbon export from the Mississippi River Basin. *Global Biogeochemical Cycles*, *29*(9), 1333–1347. <https://doi.org/10.1002/2014GB005068>
- Tian, H., Xu, R., Canadell, J. G., Thompson, R. L., Winiwarter, W., Suntharalingam, P., et al. (2020). A comprehensive quantification of global nitrous oxide sources and sinks. *Nature*, *586*(7828), 248–256. <https://doi.org/10.1038/s41586-020-2780-0>
- Verpoorter, C., Kutser, T., Seekell, D. A., & Tranvik, L. J. (2014). A global inventory of lakes based on high-resolution satellite imagery. *Geophysical Research Letters*, *41*(18), 6396–6402. <https://doi.org/10.1002/2014GL060641>
- Weyhenmeyer, G. A., Meili, M., & Livingstone, D. M. (2004). Nonlinear temperature response of lake ice breakup. *Geophysical Research Letters*, *31*(7). <https://doi.org/10.1029/2004GL019530>
- Wik, M., Varner, R. K., Anthony, K. W., MacIntyre, S., & Bastviken, D. (2016). Climate-sensitive northern lakes and ponds are critical components of methane release. *Nature Geoscience*, *9*(2), 99–105. <https://doi.org/10.1038/ngeo2578>
- Wit, F., Müller, D., Baum, A., Warneke, T., Pranowo, W. S., Müller, M., & Rixen, T. (2015). The impact of disturbed peatlands on river outgassing in Southeast Asia. *Nature Communications*, *6*(1), 10155. <https://doi.org/10.1038/ncomms10155>
- Yang, X., Pavelsky, T. M., & Allen, G. H. (2020). The past and future of global river ice. *Nature*, *577*(7788), 69–73. <https://doi.org/10.1038/s41586-019-1848-1>
- Yao, Y., Tian, H., Shi, H., Pan, S., Xu, R., Pan, N., & Canadell, J. G. (2020). Increased global nitrous oxide emissions from streams and rivers in the Anthropocene. *Nature Climate Change*, *10*(2), 138–142. <https://doi.org/10.1038/s41558-019-0665-8>